Author Manuscript

Author Manuscript

Author Manuscript

Author Manuscript

HHS Public Access

Author manuscript

Biomaterials. Author manuscript; available in PMC 2016 September 21.

Published in final edited form as:

Biomaterials. 2014 March ; 35(10): 3252–3262. doi:10.1016/j.biomaterials.2013.12.093.

Enhanced reseeding of decellularized rodent lungs with mouse embryonic stem cells

Shimon Lecht[a], **Collin T. Stabler**[a], **Alexis L. Rylander**[a], **Rachel Chiaverelli**[a], **Edward S. Schulman**[b], **Cezary Marcinkiewicz**[a], and **Peter I. Lelkes**[a,*]

[a]Department of Bioengineering, College of Engineering, Temple University, Philadelphia, PA 19122, USA

[b]Division of Pulmonary, Critical Care and Sleep Medicine, Drexel University College of Medicine, Philadelphia, PA 19102, USA

Abstract

Repopulation of decellularized lung scaffolds (DLS) is limited due to alterations in the repertoire and ratios of the residual extracellular matrix (ECM) proteins, characterized by e.g., the retention of type I collagen and loss of glycoproteins. We hypothesized that pre-treatment of decellularized matrices with defined ECM proteins, which match the repertoire of integrin receptors expressed by the cells to be seeded (e.g., embryonic stem cells) can increase the efficacy of the reseeding process. To test this hypothesis, we first determined the integrin receptors profile of mouse embryonic stem cells (mESCs). Mouse ESCs express α3, α5, α6, α9 and β1, but not α1, α2 and α4 integrin subunits, as established by Western blotting and adhesion to laminin and fibronectin, but not to collagens type I and IV. Reseeding of DLS with mESCs was inefficient (6.9 ± 0.5%), but was significantly enhanced (2.3 ± 0.1 fold) by pre-treating the scaffolds with media conditioned by A549 human lung adenocarcinoma cells, which we found to contain ~5 μg/ml laminin. Furthermore, pre-treatment with A549-conditioned media resulted in a significantly more uniform distribution of the seeded mESCs throughout the engineered organ as compared to untreated DLS. Our study may advance whole lung engineering by stressing the importance of matching the integrin receptor repertoire of the seeded cells and the cell binding motifs of DLS.

Keywords

Acellular matrix; Cell adhesion; Embryonic stem cells; Extracellular matrix (ECM); Integrin; Lung

1. Introduction

Lung diseases are a significant cause of morbidity and mortality worldwide. Approximately 3500 lung transplantations per year are performed worldwide [1]. The shortage of suitable

*Corresponding author. Temple University, Engineering Building, Room 811, 1947 N. 12th Street, Philadelphia, PA 19122, USA. Tel.: +1 215 204 3307; fax: +1 215 204 3326. pilelkes@temple.edu (P.I. Lelkes).

Disclosure statement

No competing financial interests exist.

Author Manuscript Author Manuscript Author Manuscript Author Manuscript

donor lungs for transplantation emphasizes the need for other therapeutic approaches, such as cell-based regenerative therapies [2]. Amongst the possible solutions is the transplantation of engineered decellularized/repopulated lungs [2]. Different decellularization methodologies have been developed for efficient lysis and removal of cells, ranging from physical methods such as repeated freezing and thawing, to the use of chemical (e.g., detergents) and biological (e.g., enzymes) agents as single approaches or in combination [3]. Decellularized scaffolds then serve as matrices for recellularization using a variety of cell types e.g., repopulating the decellularized lung scaffolds (DLS) using whole lung cell suspensions, endogenous progenitor cells, embryonic/adult stem cells and induced pluripotent stem cells at different stages of differentiation [4]. Decellularization of the lung results in a cell-free, acellular, 3-dimensional (3-D) extracellular matrix (ECM) scaffold, which retains the gross anatomy of the original tissue/organ, but differs from the native lung ECM, in terms of protein composition, ultrastructure and mechanical properties [5]. It is becoming increasingly evident that the altered physicochemical properties of the DLS are in part responsible for the limited efficacy of recellularization [2]. The lack of efficiency and ability to fine-tune the recellularization process is of concern for translating this decellularization/recellularization technology of whole functional organ engineering into future clinical use.

Integrin receptors provide the primary functional link between cells and ECM components, thus mediating specific adhesion, physical and topographic sensing of the substratum [6]. Integrin receptors are heterodimers of α and β subunits, which responsible for the receptoral specificity through varying combination of currently identified 18 α and 8 β subunits [7]. In general, each cell type expresses a unique profile of integrin receptors that undergo dynamic changes e.g., during ESCs differentiation [8]. Therefore, a potential approach to improving the recellularization process is to characterize the integrin receptors profile of reseeded cells and in parallel, to restore some of the components of the decellularized lung ECM, which were lost during the decellularization process in order to enhance adhesion, spreading and site-specific differentiation of the reseeded cells. We hypothesized that pre-treatment of DLS with defined ECM proteins that match the repertoire of integrin receptors expressed by the cells to be seeded (e.g., embryonic stem cells) can increase the efficacy of the reseeding process. This approach has not yet been quantitatively addressed in the context of cell–biomaterial interactions in lung tissue engineering.

To test our working hypothesis we pre-treated decellularized lung scaffolds with conditioned media (CM) of A549 cells, a human alveolar adenocarcinoma cell line, which contains a number of lung-specific ECM proteins, such as laminin (LM) and fibronectin (FN) [9]. The A549-CM is also of particular interest, because it induces pulmonary differentiation of mouse embryonic stem cells (mESCs), as previously shown by our laboratory [10] and others [11].

2. Materials and methods

2.1. Embryonic stem cell culture

Mouse embryonic stem cells, E14tg2a (ATCC CRL-1821) were originally purchased from ATCC (Manassas, VA). For comparison, another batch of the same cells was kindly

Author Manuscript Author Manuscript Author Manuscript Author Manuscript

provided by Prof. Athanasios Mantalaris (Biological Systems Engineering Laboratory, Imperial College, London, UK). No differences were noted between the two sets of cells. The cells were maintained in a feeder-free culture system in T-75 tissue culture flasks coated with 0.1% gelatin (Millipore, Billerica, MA) in a humidified incubator at 37 °C in 5% CO_2. The maintenance media was composed of Dulbecco's Modified Eagle Medium (DMEM, Cellgro, Manassas, VA) supplemented with 10% stem-cell grade FBS (Biowest, France), 100 IU/ml penicillin and 100 μg/ml streptomycin (Cellgro), 2 mM L-Glutamine (Invitrogen, Carlsbad, CA), 10 ng/ml human recombinant BMP-4 (R&D Systems, Minneapolis, MN), 1000 U/ml ESGRO® mouse LIF (Millipore) and 0.15 mM 1-Thioglycerol (Sigma, St. Louis, MO), as previously described [11]. The maintenance media was changed every day and cells were split every 2–3 days using trypsin (TrypLE Express, Invitrogen) upon reaching 80% confluence at a 1:6 ratio. The cell cultures were routinely visually evaluated and microphotographs were taken using a Nikon Eclipse TE 2000-U (Nikon, Melville, NY) connected to a Hitachi KP-D50 digital camera (Woodbury, NY).

2.2. Preparation of conditioned media

A549 cells (ATCC CCL-185) were cultured in T-150 tissue culture flasks in a humidified incubator at 37 °C in a 5% CO_2 atmosphere. The cells were maintained in DMEM (Cellgro) supplemented with 10% FBS (Gemini BenchMark, West Sacramento, CA), 100 IU/ml penicillin and 100 μg/ml streptomycin (Cellgro), and 2 mM L-Glutamine (Invitrogen). The maintenance media was changed every other day and the cells were split upon reaching 80% confluence at a 1:8 ratio using trypsin (TrypLE Express, Invitrogen) as previously described [10]. In order to collect serum-free conditioned media (CM), 90% confluent flasks were quickly washed three times with Hank's Balanced Salt Solution (HBSS, Cellgro) containing calcium and magnesium followed by three additional washes for 10 min each with serum-free DMEM supplemented with antibiotics. To initiate CM collection each flask was supplemented with 30 ml of serum-free DMEM containing antibiotics and left for 48 h in the incubator. Upon completion of the conditioning step, the CM was collected and filtered through sterile low protein binding 0.2 μm syringe filters (Corning, Corning, NY). The filtered CM (considered as 100% CM) was aliquoted and kept at −20 °C. Aliquots were thawed only once immediately before use.

2.3. Immobilization of proteins for adhesion and ELISA assays

For the adhesion assays, compounds of interest (select ECM proteins, purified disintegrins, integrin receptor-specific antibodies, DMEM and CM) were immobilized in the wells of 96 well ELISA plates with high binding surface capacity (Cat. No.: 3590; Corning) and incubated overnight at 4 °C. The following ECM proteins were immobilized in a volume of 100 μl/well at a concentration of 10 μg/ml in phosphate buffered saline (PBS, Cellgro): bovine collagen type IV (Millipore); human collagen type IV (Millipore); human pro-collagen type I (kind gift from Dr. Andrzej Fertala, Thomas Jefferson University, Philadelphia, PA, USA); human collagen type I (Millipore); rat collagen type I (BD Biosciences, San Jose, CA); human plasma-purified fibronectin (Millipore); thrombospondin-1 (purified from human platelets [12]); VCAM (R&D Systems, Minneapolis, MN); vitronectin (R&D Systems); bovine elastin (sigma); Matrigel-purified laminin 111 (Sigma); and human recombinant laminins 111, 211, 332, 411, 421, 511, 521

Author Manuscript Author Manuscript Author Manuscript Author Manuscript

(BioLamina, Sweden). The following disintegrins were purified from lyophilized snake venoms as previously described [7] and immobilized in a volume of 100 µl/well at a concentration of 20 µg/ml in PBS: viperistatin; VP-12; VLO-4, VLO-5 and echistatin. The antibodies were immobilized in a volume of 100 µl/well at a concentration of 10 µg/ml in PBS (listed in S-Table 1). Different concentrations of CM diluted with DMEM were immobilized at a final volume of 100 µl/well overnight at 4 °C. As negative controls PBS-only, DMEM-only and 10 µg/ml of BSA (Sigma), were immobilized overnight at 4 °C in a final volume of 100 µl/well.

In order to co-immobilize multiple ECM proteins, following the first immobilization step, as described above, the wells were washed three times with 200 µl Hank's Balanced Salt Solution (HBSS) without Ca^{2+} and Mg^{+2}, and incubated with 200 µl/well of 1 mg/ml BSA (1% BSA blocking solution) for 1 h at room temperature (RT). Thereafter, the wells were washed three times with 200 µl HBSS without Ca^{2+} and Mg^{+2}, and incubated with 1 µg/well of fibronectin or laminin, or 100 µl/well of 100%-CM for 1 h at 37 °C. As negative controls, immobilized BSA (1 µg/well) was incubated with 1 µg/well fibronectin or laminin, or 100%-CM for 1 h at 37 °C at a final volume of 100 µl/well.

2.4. Adhesion assay

The adhesion assay was based on a previously published protocol [13] with specific adjustments for mESCs. Upon completion of the immobilization step, as detailed above, the wells were quickly washed three times with 200 µl HBSS without Ca^{2+} and Mg^{+2}, and incubated for 1 h at RT with 200 µl/well of 1% BSA in HBSS (blocking solution) to block non-specific binding sites. In parallel, subconfluent mESCs cultures were washed three times with HBSS without Ca^{2+} and Mg^{+2}, trypsinized and centrifuged for 5 min at 1000 RPM. The cell pellet was resuspended in 1 ml of HBSS with Ca^{2+} and Mg^{+2}, The vital fluorescent probe CellTracker™ Green 5-Chloromethylfluorescein Diacetate (CMFDA, Invitrogen) was added at final concentration of 5 µg/ml and incubated for 30 min at 37 °C. Only viable cells enzymatically cleave the non-fluorescent molecule to produce a cell membrane impermeable fluorescent product. The stock solution of CMFDA was prepared in dimethyl sulfoxide (DMSO; Sigma) and the final concentration of DMSO in the cell suspension never exceeded 0.1%. Thereafter, the labeled cell suspension was diluted with blocking solution and centrifuged for 5 min at 1000 RPM. The pellet was resuspended, counted and diluted in blocking solution to a final cell concentration of 1×10^6 cells/ml. To initiate the adhesion assay, 100 µl of cell suspension were added to each well and incubated for 1 h at 37 °C. Thereafter, the wells were washed quickly three times with 200 µl/well of blocking solution. The specifically attached cells were solubilized in 100 µl/well of 0.5% Triton X-100 (Sigma). In order to estimate the number of attached cells, a calibration curve was prepared by solubilizing increasing volumes of the cell stock suspension (containing known cell numbers) with 100 µl/well of 0.5% Triton X-100. For each experiment a new calibration curve was generated, which included at least six different points in duplicates and resulted in linear correlation coefficient ($R^2 > 0.95$) between cell-associated fluorescence and cell number. Upon solubilization, the fluorescence of the well was quantified using a fluorescence plate reader (Synergy-4, Biotek, Winooski, VT) at λ_{Ex} = 485 nm/ λ_{Em} = 528 nm. The number of attached cells was calculated from the calibration curve and expressed as

Author Manuscript Author Manuscript Author Manuscript Author Manuscript

percentage of adhesion to 1 μg/well of fibronectin, which was considered as positive control, unless mentioned otherwise.

2.5. Western blotting

Isolation of total cellular proteins, protein quantitation and Western blotting were performed essentially as previously described [14]. Briefly, subconfluent cultures of mESCs were scraped on ice and lysed with RIPA lysis buffer (Teknova, Hollister, CA). The amount of total soluble protein was quantified using the BCA protein assay (Pierce, Rockford, IL). For Western blotting, aliquots of protein solutions were mixed with β-mercaptoethanol-containing Laemmli sample buffer (Bio-Rad, Hercules, CA) at a ratio of 2:1, denatured for 5 min at 95 °C and a final amount of 35 μg protein was loaded onto 4–15% precast mini-polyacrylamide gradient gels (Bio-Rad). The samples were separated by SDS-PAGE (100 V for 1.5 h) and transferred for 30 min at 25 V using a semi-dry blotting system (Bio-Rad) to PVDF membranes (Millipore). The non-specific binding was blocked for 2 h at RT using 5% non-fat powdered milk (Santa-Cruz, Dallas, TX) and incubated with primary antibodies (listed in S-Table 1) at 4 °C overnight. The next day, detection was performed using horseradish-peroxidase-conjugated secondary antibodies (listed in S-Table 1) and visualized by chemiluminescence using an ECL 2 Western Blotting Substrate (Pierce). Subsequently, the membranes were stripped using Restore Western Blot Stripping Buffer (Pierce) and incubated with an anti-actin antibody as a control for equal protein loading. Films were exposed between 5 and 60 s, developed and scanned in a flat-bed scanner in transmission mode (Epson, Long Beach, CA). Positive controls for integrin receptors included 35 μg of total protein from K562 cells for α5 (ATCC CCL-243), K562 cells overexpressing α2 or α6 (kind gift from Dr. Martin E. Hemler, Dana-Farber Cancer Institute, Boston, MA, USA), A549 cells for α1 and α3, and LN229 cells for α9 and αV (ATCC CRL 2611).

For detection of proteins in the CM, aliquots of three independently collected batches were mixed with β-mercaptoethanol-containing Laemmli sample buffer at a 3:1 ratio and denatured for 5 min at 95 °C. A final volume representing 30 μl of CM was loaded on precast mini-polyacrylamide 4–15% gradient gels, separated, transferred and processed as described for total cellular protein. As positive controls for identifying ECM proteins in the CM, the same purified proteins that were used during immobilization for the adhesion assay were also loaded on gels at 1 μg/lane. Molecular weights of the resolved proteins in each gel electrophoresis were assessed using Novex size markers (Invitrogen).

2.6. ELISA of ECM proteins in CM

Immobilization of proteins for ELISA was performed similarly as for adhesion assay (see above) with the exception that the volume of the immobilized proteins in each well was 75 μl. Each ELISA experiment included a calibration curve composed of 7 serial three-fold dilutions in duplicates as previously described [15]. Briefly, upon completion of the immobilization step the wells were quickly washed three times with 200 μl PBS supplemented with 0.05% Tween-20 (PBST), blocked for 1 h at 37 °C with 200 μl/well of 5% non-fat dry milk in PBST and incubated for 1 h at 37 °C with 100 μl of primaryantibodies (listed in S-Table 1) diluted in 3% non-fat dry milk in PBST. Upon completion of the incubation with primary antibody, the wells were quickly washed three

Author Manuscript Author Manuscript Author Manuscript Author Manuscript

times with 200 μl PBST, incubated for 1 h at 37 °C with 100 μl of alkaline phosphatase (ALP)-conjugated secondary antibody (listed in S-Table 1) added in 3% non-fat dry and developed using 100 μl of the colorimetric ELISA assay ALP substrate (Sigma) at RT. Colorimetric development was monitored by measuring absorbance at 405 nm and terminated when all seven points of the calibration curves were successfully developed. All ELISA experiments contained also control wells, where the primary antibody was omitted, while the other steps remained unchanged.

In order to quantitatively analyze the ELISA assays, calibration curves were fitted using the four parameters logistic nonlinear regression model (SigmaPlot v.10, Systat Software Inc., San Jose, CA). Experiments with correlation coefficients for the calibration curve of $R^2 < 0.95$ were discarded. Experiments in which the absorbance values for the "unknown" samples had OD signals higher than the upper detection limit were repeated with serial dilutions of the "unknown" to achieve a result in the detection range. Results showing values below the detection limit were considered as 0 (or ND –not detected).

2.7. Lung de-cellularization

The decellularization process of rat lungs was performed in part according to a protocol previously developed and extensively validated in our laboratory [16]. Whole hearts and lungs were surgically removed *en-bloc* immediately upon sacrifice of adult male or female Sprague Dawley rats (Taconic Farms Inc., Hudson, NY) that had served as normal control animals in unrelated research protocols. The removed lung-heart preparations were cleaned of loose connective tissue and rinsed repeatedly in calcium/magnesium free phosphate buffered saline (PBS) (Life Technologies Grand Island, NY) supplemented with antibiotics. From this point forward, aseptic techniques were followed. The isolated organs were initially placed at a volume ratio of ~1:8 in a solution of 4% sodium deoxycholate (SDC; Sigma) and 3% Triton X-100 (Millipore) prepared using deionized distilled water (pH of 7.4) in 50 ml centrifuge tubes. The tubes were placed in a slowly moving (5 RPM) rotary carousel hybridization oven (Labnet, Edison, NJ) at 37 °C, where they were kept for the whole duration of the decellularization protocol. The decellularization solution was exchanged daily with incrementally diluted detergent solutions, i.e., the concentration of both detergents was reduced by 0.5%/day. The concentration of Triton X-100 was eventually kept constant at 0.5% until the concentration of SDC had also reached 0.5% (by day 6 of protocol). Following detergent decellularization, the tissues were immersed 3 times for 5 min each in PBS and remained in fresh PBS overnight at 4 °C. Next, the tissues were immersed in a 1% solution of DNA-away (Molecular BioProducts Inc., San Diego, CA) in distilled water for 2 h at RT followed by overnight incubation in 0.2% DNAse solution (Millipore) at 4 °C. Thereafter, the decellularized lungs were immersed 3 times for 5 min each in PBS and incubated overnight in fresh PBS at 4 °C. To monitor the progress of the decellularization process, some sample tissues were subjected to total DNA extraction (according to manufacturer's instructions; Omega biotek, Norcross, GA) on a daily basis until no DNA was detected by the end of the decellularization process. The organs were kept in DMEM supplemented with 10% ABAM (antibiotic/antimycotic solution, from Mediatech Inc.) at 4 °C. The decellularized organs were stored for no longer than two weeks prior to

Author Manuscript Author Manuscript Author Manuscript Author Manuscript

use, the storage media was occasionally evaluated for the absence of bacterial contamination.

2.8. Recellularization of decellularized lungs

Only the left lobe was used for recellularization experiments, while the right main bronchus was tied twice with 3–0 silk surgical suture. An 18G iv catheter was inserted through the trachea passing the carina until the left main bronchus was reached, as ascertained by visual inspection. The catheter was then tied around the trachea with 3–0 silk surgical suture to secure its placement. To validate tight closure of the sutures, the lungs were gravitationally inflated with 10 ml of the storage solution resulting in inflation of the left lobe only and lack of inflation of the right lobes. Prior to recellularization, the left lobe was coated by gravitational inflation with 10 ml of A549-CM, allowing the lobe to recoil in a cylindrical tube containing 25 ml of the CM followed by overnight incubation at 4 °C. On the next day, the lungs were re-warmed (37 °C for 1 h) prior to introducing the cells. As negative controls, same coating procedure was performed using DMEM-only.

In order to quantitatively analyze the regional seeding efficiency in the recellularized left lung, mESCs were labeled with CMFDA as described above (see Section 2.4). The left lobe was recellularized by gravitational inoculation using 10×10^6 CMFDA-labeled mESCs suspended in 10 ml of DMEM or A549-CM. The reseeded lobe was incubated at 37 °C for 1 h to allow cell adhesion to the matrix. In order to quantitate specificallyadheredcells only, followingreseeding the unattachedcells were washed in 5 cycles of slow horizontal inflation with 10 ml PBS and full spontaneous recoiling.

2.9. Quantitation of cells in recellularized lungs

Following recellularization, the left lobe was dissected from the heart-lung preparation and sliced horizontally along the vertical axis using a surgical razor blade thus generating (in a cranial to caudal direction) five equal macro-slices: slice 1–apex of the lobe; slice 2–main left bronchus entrance with small margins above and below the orifice; slices 3–5–three sequential slices of similar width starting below the orifice of the main left bronchus and progressing towards the caudal end of the lobe (see schematic drawing in Fig. 5). The macro-slices were placed in 1.5 ml centrifuge tubes and solubilized in 300 μl of 0.1% Triton-X 100 overnight with orbital shaking (100 RPM) at RT in order to extract the fluorescent label from the cells present in the macro-slices. The extracted CMFDA fluorescence was measured in a fluorescent microplate reader (Synergy-4, Biotek) and the cell number was calculated using a calibration curve of labeled cells solubilized in 1.5 ml tubes following similar procedures as for the macro-slices. Decellularized lungs without cell inoculation were subjected to a similar solubilization procedure and the intrinsic auto-fluorescence was used as background. In order to compensate for possible differences in the sizes of the macro-slices, upon solubilization the macri-slices were transferred to the pre-weighted tubes and dried overnight using speed-vac (Thermo, Waltham, MA). The number of reseeded cells in each macro-slice was normalized to mg dry weight of each sample.

In another approach to quantitate the cells in the reseeded scaffolds, we prepared histological slides from tissues sectioned at the apex, mid and base locations of the lung. Phase-contrast

Author Manuscript Author Manuscript Author Manuscript Author Manuscript

and DAPI-stained micrographs were taken using an Olympus FSX-100 fluorescent microscope using 4.2× objective and stitched to represent the whole tissue slice. To count the cells number and to generate density maps we used a combination of two open-source image analysis plug-ins “Patch Detector Plus” and “3D surface plot,” respectively, in ImageJ software (ver. 1.45s, NIH). To calculate the spatial distribution of cell densities, the whole slice was overlaid with a grid where each field was equivalent to 114,255 μm^2. This area corresponds to a cross-cut area of 15 alveoli assuming an average rat alveolus diameter of 47.6 μm [17]. Since histological sections are nearly impossible to prepare with having all alveoli aligned on the same plane, the area representing 15 alveoli was chosen to minimize the inherent systemic errors in image analysis due to intra-and inter- sample variability in image alignment. The average number of analyzed fields was on apex–169; mid–459; base–222.

2.10. Preparation of tissue slides

The left lobes were fixed via intratracheal gravitational instillation of 10 ml of 10% buffered Formalin (Azer Scientific, Morgantown, PA) followed by immersion into the same fixative for at least 24 h at 4 °C. The tissue was cut into 3 mm sections at the apex, mid, and base portions (see schematic drawing in Fig. 6) followed by dehydration through an ethanol gradient with 30 min steps: 40, 60, 80, 90, 95, 100% 190-proof ethanol (Decon Laboratories), 100% 200-proof ethanol (Pharmco-AAPER, Kindermorgan, PA), and then cleared with two changes of 100% Substitute (Thermo) for 1 h each. These tissue sections were then embedded in molten paraffin (Fisher Scientific) at 60 °C, with 2 changes for 2 h each, and placed into blocks. Thin sections (5 μm thickness) were prepared using a Leica RM2255 microtome (Leica, Germany) and collected onto positively charged microscope slides (VWR, Radnor, PA). The samples were dried overnight and re-hydrated by two 10 min changes of Xylene Substitute, a 10 min change of Xylene/190-proof ethanol at 1:1 ratio, followed by 10 min changes of 100, 100, 90, 80, 70% 190-proof ethanol and, finally, deionized water. For assessing cell numbers, the slides were then mounted with DAPI-containing VectaShield (Vector Laboratories, Burlingame, CA), covered with coverslips and sealed with nail polish. Slides were kept at 4 °C until imaging.

2.11. Statistical analyses

Each experiment was independently repeated at least 3–5 times in triplicates ($n = 9–15$), unless otherwise specified. The results are presented as the mean ± SEM when applicable. Statistically significant differences between experimental groups were determined by analysis of variance test (ANOVA) followed by Bonferroni post-test, unless mentioned otherwise, using the InStat statistics program (GraphPad, La Jolla, CA). Significance was set for $p < 0.05$.

3. Results

3.1. Characterization of integrin receptor-mediated adhesive properties of CM

Analysis of A549-derived CM using Western blotting revealed the presence of laminin (LM), fibronectin (FN), collagen type IV (Coll IV) and thrombospondin-1 (TSP-1), while vitronectin (VT) and collagen type I (Coll I) were undetectable (Fig. 1A). In a

Author Manuscript Author Manuscript Author Manuscript Author Manuscript

complementary quantitative approach by ELISA (S-Fig. 1), the following amounts of ECM proteins were found in the CM: Coll IV: 13.1 ± 5.9 ng/ml; TSP-1: 34.3 ± 1.3 ng/ml; FN: 42.8 ± 3.3 ng/ml; and, remarkably, copious amounts of LM: 5309.3 ± 406.4 ng/ml; Coll I and VT were again undetectable. To test the functional activity of CM-derived ECM proteins we utilized an established adhesion assay (see M&M, Section 2.4). The total CM, immobilized on high binding surface multi-well plates, exhibited a dose-dependent adhesion of mESCs with an EC_{50} of 8.9 ± 0.3% of CM and an efficacy of 95.5 ± 0.1% (Fig. 1B).

In confirming and extending our previous studies, in which we characterized the integrin receptor profile in mESCs using ES-D3 cells [18], we now examined the integrin profile of E14tg2a cells, a frequently used mESCs line [19]. As depicted in Fig. 2A, E14tg2a cells expressed α3, α5, α6, α9, αV and β1 integrin subunits, while α1, α2 and α4 subunits were not identified. To validate the functionality of the mESC-expressed integrin receptors, we tested adhesion to their endogenous ligands (Fig. 2B). E14tg2a mESCs adhered preferentially to FN (100.0 ± 2.0%) and LM (83.7 ± 3.1%), and to a lesser extent also to TSP-1 (20.8 ± 2.8%), VCAM (26.9 ± 3.0%) and VT (22.4 ± 1.8%), which interact with the subunits α5 (FN), α3/α6 (LM), α9 (TSP-1), α4/α9 (VCAM) and αV (VT), but not to Coll IV or I, as also expected from the absence of α1 and α2 subunits, respectively. The absence of α1, α2 and α4 expression was further confirmed using adhesion assays on immobilized specific antibodies (S-Fig. 2A) and immobilized integrin-specific disintegrins/antagonists [18] (S-Fig. 2B). The results of adhesion to immobilized antibodies and disintegrins, independently confirmed the absence of functional α1 and α2 and the presence of functional α5, α9 and αV subunits. Considering that the adhesion to immobilized ligands depends on the expression levels of functional integrin receptors on the cell surface, we conclude that α5β1 and α3β1/α6β1 are the most abundant integrin receptors expressed by the mESCs.

In the next series of experiments, we measured the adhesion of mESCs to immobilized purified ECM proteins and found that the cells adhered in a dose-dependent manner to LMs, FN, VT and TSP-1 (S-Fig. 3) with potency and efficacy values as listed in Table 1. Laminin next to FN appears to be the major pro-adhesive ECM protein for mESCs. Since LM exists in mammalian tissues in variety of isoforms [20], which may have different affinity towards mESCs adhesion, we next evaluated a series of recombinant LMs representing the diversity of isoforms present in the lung [20]. The mESCs were found to adhere differentially in an isoform-dependent manner with the following order of potencies LM 511 = 521 >332>421 > 211>111 >411 (Table 1 and S-Fig. 3). These findings further support the notion that α3β1 and α6β1 integrin receptors expressed on the mES cell surface are involved in the specific binding to LM in general and to LM 511 in particular, which is the major LM species found in A549-CM [21,22].

3.2. Quantitative analysis of CM-derived ECM–ECM protein interactions in vitro and in decellularized lungs

Collagens are the major ECM proteins in normal lung [23]. In decellularized lungs the relative presence of Coll I/IV is further enriched, irrespective of the decellularization technique used [24]. However, mESCs lack expression of the α1 and α2 integrin subunits and are therefore unable to adhere to Coll IV and I, respectively (Fig. 2). On the other hand,

Author Manuscript Author Manuscript Author Manuscript Author Manuscript

it is well established that ECM components generate complex matrix structures both *in situ* and *in vitro*, due to heterotypic molecular/biochemical interactions, in particular between collagens and LM and FN [25]. In the next series of experiments we tested whether addition of A549-CM would result in formation of molecular complexes between CM-derived LM and FN with the abundant ECM proteins in the lung (collagen type I, IV and elastin) and ultimately improve indirect mESC adhesion to these otherwise non-permissive proteins. We fist immobilized Coll IV, Coll I and elastin and, after blocking, incubated the wells with 1 μg/ml FN, LM or 100% CM. Adhesion of mESCs to Coll I, but not Coll IV or elastin, was dramatically increased upon pre-treatment with FN or LM (Fig. 3). Pre-treatment of Coll I with CM was even more effective, significantly increasing mESC adhesion by 19% and 35% above FN and LM alone, respectively. The pro-adhesive effect of the CM was also evident upon pre-treatment of Coll IV, albeit only to a much lower degree. CM treatment had no effect on mESC adhesion to elastin, similarly to pre-coating with LM or FN alone (Fig. 3). These findings indicate that increased adhesion of mESCs to Coll I/IV pre-treated with CM is most probably the result of molecular interactions between CM-derived FN/LM and Coll I/IV [25]. These molecular interactions were further quantitated using “sandwich-like” ELISA assays to measure the extent of interaction of LM and FN with Coll IV, Coll I and elastin. Our data suggest a significantly higher efficiency of interaction between CM-derived LM and FN with immobilized collagens as compared to purified individual LM and FN (S-Table 2), which is also reflected in the significantly enhanced adhesion of mESCs to the CM-derived ECM/collagens protein complexes (Fig. 3 and S-Fig. 4).

In the next series of experiments we tested *ex vivo* the efficacy of our “pre-treatment with CM” approach using DLS. Complete decellularization was confirmed by the absence of DNA (0 ng/mg tissue) and negative DAPI staining (S-Fig. 5A,B) and maintenance of a structural integrity similar to that of native lungs (S-Fig. 5C,D). Given the interactions between CM-derived LM/FN and collagens as demonstrated above, and because decellularized lungs are enriched in collagens, especially Coll I [24,26], we hypothesized that the collagens in the DLS might be accessible for such interactions and adsorb significant amounts of CM-derived ECM proteins, specifically LM and FN. To test this hypothesis, we quantified the amounts of ECM proteins removed from the CM after incubation with decellularized lung slices. The decellularized lung slices were able to adsorb 45 ± 6% of total available LM or FN in CM, specifically 2900 ± 900 ng LM and 58 ± 16 ng FN per mg dry lung scaffold (Fig. 4A).

Based on the indication that ECM proteins are removed from the CM and adsorbed to the decellularized lung slices we incubated the left lobes of the decellularized lungs upon inflation with 10 ml of either DMEM or CM. Thereafter, we intratracheally inoculated fluorescently-labeled mESCs into the left lobes of DLS and measured, after 1 h, the number of retained cells by extracting the fluorescent markers from the whole left lobe. Overall, lobes pre-treated with CM exhibited a 2.3 ± 0.1-fold increase in the number of retained cells as compared to DMEM-treated control group (Fig. 4B).

Author Manuscript Author Manuscript Author Manuscript Author Manuscript

3.3. Quantitative analysis of spatial distribution of mESCs reseeded into CM-treated decellularized lungs

Enhanced reseeding of DLS requires not only more efficient repopulation, i.e., larger numbers of cells retained, but also a more uniform distribution throughout the organ. The 3D structure of lungs is quite complex due to bifurcating airways with lack of systematic directionality [27]. Therefore, upon reseeding DLS, we sought to quantitatively analyze the spatial distribution of inoculated cells. To reseed the decellularized lung, the right main bronchus was ligated and the mESCs were inoculated intratracheally into the left lobe only, as described above (M&M, Section 2.8). Fig. 5A schematically depicts our approach for quantitation of specifically adhered cells. The left lobe was cut into five pieces, along the vertical axis (cranial-caudal, *z*-axis), followed by quantitation of the number of adhered cells. The pre-treatment of the decellularized lung matrix with CM resulted in significantly more homogeneous distribution along the vertical axis of the lobe as compared to DMEM-treated control lobes (Fig. 5B). In DMEM-treated lobes, the mESCs were overwhelmingly localized in the central part of the lobe (slice 3 in Fig. 5B). However, in CM pre-treated lobes, the mESCs had a more uniform distribution along the cranial-caudal (*z*-) axis with the only exception of the apex area (Fig. 5B).

In further evaluating mESCs reseeding in CM-treated decellularized lungs, we analyzed cellular distribution along the horizontal plane (ventral-dorsal *x*–*y* plane). Histological slides were prepared of transverse sections from the apex, mid and base areas (Fig. 6A). These histological slices were photographed at low magnification/ high resolution in a stitching microscope and overlaid with a grid where each square is of 114,255 μm^2, representing a cross-sectional area of 15 alveoli, as described above in the M&M section (see Section 2.9). We first analyzed, as a reference point, native normal rat lungs and calculated an averaged cell density of 6.2 ± 0.6 cells/ alveolus throughout apex, mid and base areas (Fig. 6B and S-Fig. 6). Overall, the CM-treated lobes exhibited a more uniform longitudinal cell density distribution calculated as 1.8 ± 0.1 and 1.3 ± 0.1 cells per alveolus in the mid and base area (Fig. 6B). Lung lobes, pre-treated with DMEM, contained 2.8 ± 0.2 cells per alveolus in the mid area and exhibited very low density of 0.31 ± 0.03 cells per alveolus at the base area. The density of the cells in apex area in the CM-treated lobes was still low, although 3-fold higher than in the DMEM-treated control lobes, with 0.25 ± 0.05 and 0.08 ± 0.02 cells per alveolus, respectively (Fig. 6B). The similarity of the cell densities between mid and base areas of CM-treated DLS, the low density in the apex areas and the exacerbated accumulation of cells in the mid area of DMEM-treated DLS are in line with the longitudinal fluorescence extraction assay (Fig. 5). Taken together, these results support our notion that pre-treatment of decellularized rat lung scaffolds with A549-CM leads to enhanced repopulation with mESCs and more uniform distribution across the tissue. The calculation of cell density is an important parameter for the estimation of pre-treatment efficiency but provides only limited information about the cell distribution on the whole organ level. Since lungs have a highly complex planar structure, we further attempted to estimate the uniformity of cell densities in each slide and calculated the variation of cell density distribution across the horizontal plane (transverse sections) using coefficient of variance (%CV) derived from averaged cell density (Fig. 6C). In the normal native rat lung the %CV at the apex, mid and base areas is on average ~42%, (Fig. 6C and S-Fig. 6). In the

Author Manuscript Author Manuscript Author Manuscript Author Manuscript

decellularized lungs, the %CV of the cell density distribution is very high at the apex and decreased in the CM-coated lobes along the *z*-axis, (Fig. 6C, D), indicating an increased uniformity in cell distribution from the apex to the base. Although in the DMEM-treated control lobes the % CV decreases as well, the CM-coated lobes displayed a significantly more uniform cell distribution in the mid and base areas (Fig. 6C, D). In view of more inhomogeneous reseeding of the DMEM-treated decellularized lobes, our results clearly emphasize the importance of CM pre-treatment towards optimization of uniformity of cell distribution. Cumulatively, our analysis of cell distribution, both horizontally and longitudinally, indicates that upon CM treatment the number of retained cells is increased and their distribution is more uniform than in the decellularized controls lungs treated with DMEM only.

4. Discussion

Decellularization provides a unique opportunity for engineering 3-D scaffolds that structurally recapitulate the complex architecture of whole organs, specifically that of lungs [28]. However, upon decellularization the remaining tissue matrices present an altered composition of ECM proteins, which in turn may hinder efficient recellularization [3]. In this study we introduce a new rational approach for functionalizing the DLS for improved recellularization. Considering that efficient and uniform initial adhesion of the seeded cells is an important prerequisite for the optimized repopulation of the decellularized matrix, we first characterized the integrin receptor profile of the model cells to be seeded (in this case E14tg2a mESCs). We demonstrated by several independent assays that mESCs lack major integrin receptors for collagens but express high levels of functional receptors for LM and FN. Thereafter, we leveraged these findings to enrich DLS with naturally occurring LM and FN in A549-CM. Both these ECM proteins, as found in the CM, were more efficacious in promoting mESC adhesion than their commercially counterparts. The coating of DLS with A549-CM significantly increased both the efficiency of mESC seeding in terms of initial adhesion and the uniformity of their spatial distribution.

All current decellularization methodologies result in significant alterations of the contents, and ratios of ECM proteins, though the exact degree of the loss of ECM glycoproteins, such as collagens, laminins, fibronectin, elastin and sulfated glycosaminoglycans (GAGs) depends to some extent on the specific decellularization protocol [3]. Overall, the capacity for ligand-receptor specific adhesion to decellularized scaffolds, which is largely determined by interactions between glycoproteins/GAG in the ECM and respective integrin receptors on the cell surface, is diminished as compared to native ECM [3]. Integrin receptors play a major role in the initial interactions between cells and biomaterials, thus their presence is crucial for functional adhesion to particular ECM proteins [29]. In order to address these issues, we first characterized the integrin receptor profile of naïve mESCs (E14tg2a line) and found expression of α3, α5, α6, α9, αV, and β1, but not α1 and α2 integrin subunits. In other words, these cells express the major integrin receptors for laminin (α3β1 and α6β1) and fibronectin (α5β1), but lack the most common integrin receptors for collagen type IV (α1β1) and I (α2β1) (Fig. 2 and S-Fig. 2). These data confirm and extend, at the protein level, the integrin expression profiles of mESCs previously demonstrated primarily at the gene level for the E14tg2a cells [30] and ES-D3 cells [18,31]. This characterization further

Author Manuscript Author Manuscript Author Manuscript Author Manuscript

suggests that efficient interactions between mESCs and the decellularized lung matrix will be mediated by α3, α5, α6, α9 and/or αV, and require the presence of ligands to these integrins, e.g., laminin and fibronectin, rather than the collagens. In decellularized lungs, type I collagen seems to be highly enriched as a result of its innate resistance to detergent-based decellularization, most probably due to its highly cross-linked triple helical structure, while other ECM components are more vulnerable to extraction or structural modification [24,26,32]. Therefore, the poor reseeding efficacy, only 6.9 ± 0.5% of the inoculated mESCs that retained in untreated DLS, is not surprising, given the fact that these cells do not express Coll I binding integrin receptors (Fig. 4B). On the other hand, we suggest that decellularized lung tissues will be an excellent seeding ground for cells expressing Coll I or IV integrin receptors.

We envision two distinct strategies for enhancing the initial reseeding efficacy: i) utilization of cells with a genetically manipulated or prior defined integrin receptor repertoire to match the ECM composition of the scaffolds to be reseeded; and/or ii) bio-mimetic functionalization of scaffolds with ECM proteins that match the endogenous set of functional integrin receptors expressed by the target cells. In view of rather rigorous regulations of potential translation into clinical setup of whole organ engineering, our tendency is to avoid genetic or other manipulations of the cells and rather modify scaffold properties to match the integrin profile of the target cells for reseeding. Based on our data on the integrin profile of mESCs and a low efficiency of the initial reseeding of decellularized lungs, we hypothesized that an un-modified lung matrix, enriched in collagens type I and IV is less conducive for efficient recellularization with mESCs, and that pre-coating of decellularized lung matrices will enhance seeding efficacy. In testing this hypothesis we evaluated the usefulness of A549-derived CM, which was previously used in a simplified onestep differentiation protocol to induce lung-specific mESCs differentiation by us [10] and others [11]. In parallel, previous studies qualitatively identified the presence of several ECM proteins in A549-CM, in particular of LM type 511 [21,22]. In this study we, for the first time, quantitated the amounts of LM and other ECM proteins in A549-CM and propose to utilize this CM as a source for pre-treating and functionalizing decellularized lung scaffold. In carefully evaluating the levels of major ECM proteins in the A549-CM we found that it reproducibly contains copious amounts of LM (~5 μg/ml) and lower levels (tens of ng/ml) of FN, Coll IV and TSP-1 (Fig. 1A). Our *in vitro* studies demonstrated a dose-dependent adhesion of mESCs to immobilized CM, suggesting that the ECM proteins in the CM preserve their bioactivity (Fig. 1B). Since collagens are enriched in decellularized lung matrices [24,26,32], we took advantage of a previously reported biochemical interaction between collagens and LM or FN [25] that, *inter alia*, leads to a switch from cell proliferation to cell differentiation [33]. We first showed *in vitro* that i) CM-derived LM and FN interact more efficiently with collagen type I (S-Fig. 4 and S-Table 2) than with collagen IV or elastin, forming a mixed complex ECM and ii) this interaction results in enhanced functional adhesion of the mESCs (Fig. 3), which lack collagen receptors (α1 and α2), but express integrin receptors for LM and FN, α3β1/α6β1 and α5β1, respectively. In addition, we demonstrated *in vitro* that CM-derived FN and LM interact with Coll I, respectively, 260 ± 6 and 48 ± 4 times more efficiently than commercial FN or LM (S-Fig. 4 and S-Table 2). This finding may be explained by a possible partial loss of activity as a result of the

Author Manuscript Author Manuscript Author Manuscript Author Manuscript

purification procedures [34], in contrast to the unprocessed CM. Therefore, for the *ex vivo* coating of DLS we utilized only A549-CM as the source for ECM proteins and not the purified proteins. We found that significant quantities of both LM and FN, ~45% of the available content in the CM, were adsorbed by the DLS, as inferred from the quantitative reduction of these proteins in the CM following pre-treatment of the decellularized lungs (Fig. 4A). Considering that collagens are the most abundant ECM proteins in the normal lung, comprising about 15% of the lung dry weight [23] and that Coll I comprises 80% of all collagens in the body, we may estimate that 12% of the lung is composed of Coll I. Thereafter, using the amount of LM adsorbed by decellularized lung (Fig. 4A) and assuming that 12% of this matrix is Coll I, we calculated that almost 90% of the available Coll I in the decellularized lung matrix forms a complex with CM-derived LM. A similar estimate for CM-derived FN yields that *ca.* 15% of Coll I is in complex with FN, suggesting that there are additional free interacting sites, which may be coated with addition of less efficient exogenous FN.

Based on the findings that CM-contained ECM proteins, in particular LM and FN, are effectively adsorbed by/to the decellularized lung matrix, we hypothesized that this biochemical interaction will lead to a significant enhancement of cell adhesion to CM-coated lung matrices during the initial reseeding with mESCs. Indeed, following pre-treatment of the decellularized lungs with A549-CM, we managed to increase the initial reseeding efficiency by 2.3-fold (Fig. 4B). The experimentally measured increase in the specific adhesion of mESCs to CM-treated lobes is in line with the predicted 2.1-fold enhancement, a number derived from estimating the expected number of adhered cell from the amounts of CM-derived LM and FN proteins adsorbed to the decellularized matrix. The close fit between experimental and predicted enhancement of cell seeding efficiency also indicates that the CM-derived ECM proteins, which are adsorbed to the lung matrix, are functional and responsible for the increased efficacy of cell adhesion, as expected and predicted from the *in vitro* experiments.

A recent study, using mESCs partially pre-differentiated into an alveolar epithelium type II (AEII) phenotype, showed no major improvement in the seeding of DLS precoated with Coll I or Matrigel [24]. This apparent lack of enhanced seeding may be in part since alveolar epithelial cells were previously shown to express integrin receptors $\alpha 3\beta 1$ and $\alpha 1\beta 1$ for LM and Coll IV, respectively, but not $\alpha 2\beta 1$ for Coll I [35]. Assuming that the integrin receptors for LM have similar affinity between mESCs and AEII, the findings in this study that Matrigel-purified LM (LM-111, [36]) is significantly less efficient in terms of cell adhesion than recombinant or A549-CM derived LM-511 may explain the lack of improvement in recellularization of Matrigel-coated DLS observed by Jensen and colleagues [24]. Our data highlight the important role of specific isoforms of LM for directed enhancement of cell adhesion to decellularized tissue matrices and the need for matching the limited repertoire of integrin receptors expressed by cells and the ECM composition of the scaffold.

To the best of our knowledge, this study is the first report to quantitatively evaluate the initial reseeding in DLS. The maximal efficiency of 16% obtained in this study, is still low by comparison to the 90% efficacy reported for decellularized liver scaffolds [37]. We attribute this limited efficacy of reseeding the lung matrix upon intratracheal instillation to the unique

Author Manuscript Author Manuscript Author Manuscript Author Manuscript

anatomical structure of airway compartment, which resembles a *cul-de-sac* organization rather than the continuously perfused vascular system, used for reseeding decellularized liver matrices. The anatomical architecture of the airways does not allow for constant unidirectional perfusion as opposed to open circular perfusable systems, such as the vascular compartment of any given organ, allowing for large volumes of cell suspensions to flow through [38]. Therefore, exposure of DLS to large volumes in order to increase the chances for circulating cell suspension to interact with ECM, may increase the recellularization capacity. We surmise that a conceptually different methodology, relying on a different set of physical and cellular parameters for efficient reseeding of the airways, has yet to be developed (these alternative approaches are currently under investigation in our laboratory).

Having improved the adhesive properties of the recellularized lung matrix and hence the seeding efficacy, we next evaluated the distribution of the cells throughout an entire reseeded lung lobe, by quantitating the density of the cells at the apex, mid and base areas of the left lung. Spatial bioimaging coupled with image analysis revealed a more uniform distribution of the reseeded cells in the CM-treated matrices than in the controls in both the longitudinal and transversal axes (Figs. 5 and 6). Decellularized lung matrix is a complex 3-D scaffold consistent of bifurcating airways that crisscross the lung in all three (*x*-, *y*-, *z*-) axes, lacking systematic directionality and exhibit increasing complexity of the airway tree with each bifurcation (generation). Previous studies in the normal naive lung indicated that upon intratracheal delivery instilled cells were localized mainly in the small airways and terminal alveoli, while cell-sized microparticles were distributed mainly in the small airways [39]. The mechanism of cell distribution in decellularized lungs scaffolds reseeded through tracheal instillation has not yet been investigated. However, with the appropriate caveats, we can draw parallels between the pulmonary distribution of instilled cells and similarly sized microparticles. Mechanisms that affect the deposition of microparticles in the lung include [40]: (i) Impaction –tendency to continue on a trajectory when the particles travel through the airway, instead of conforming to the curves of the respiratory tract; (ii) Sedimentation – physical phenomenon by which particles with sufficient mass are deposited on airways due to the force of gravity; (iii) Interception –deposition on airways walls upon initial contact, a parameter mainly depending on particle shape; (iv) Suspension –deposition due to Brownian diffusion of nanoparticles. In analogy, as a first order approximation and assuming that spherical cells are akin to microparticles, we suggest that the main mechanism that governs cell distribution in reseeded untreated decellularized lungs, is impaction mainly in area 3 (Fig. 5) and to a lower degree sedimentation in areas 4 and 5 (Fig. 5). The poor cell distribution in areas 1 and 2 may reflect the anatomical structure of the rostral part of the airway tree, since the majority of the bronchial branches split into the middle and base segments [27] as evident from noticeably less inflation in these areas of the lung during normal physiological breathing [41]. By comparing the spatial cell distribution in DMEM vs. CM-treated DLS it is tempting to propose that the observed differences are due to alteration of mechanisms of cell distribution following CM-derived ECM pre-coating. We suggest that in CM-pretreated DLS the most significant change observed in area 5 (Fig. 5) is due to a contribution of integrin receptor-mediated accelerated initial attachment and firmer adhesion of sedimented/deposited cells to suitable ECM proteins, i.e., to LM/FN instead of Coll I, which is non-adhesive for the cells used in our study. We surmise that the observed

Author Manuscript Author Manuscript Author Manuscript Author Manuscript

changes in cell retention in the different areas of the decellularized lung 1 h after cell inoculation mainly reflect initial integrin receptor-mediated adhesion. This early time point allows addressing cell adhesion in a biological system, which is dominated by specific integrin receptor-ECM interactions, rather than due to endogenous ECM synthesis and fibrillogenesis [42], or cell migration.

Whole lung lobes recellularized with different cell types were recently implanted in animal rat models as proof-of-concept to test the feasibility of bioengineering a functional whole lung [43–45]. Though these implantation studies are important milestones in pulmonary regenerative medicine, the time-limited success of these engineered organs may in part be explained by impaired recellularization, with significant areas remaining acellular or only partially populated with cells, as evident from massive edema accumulation in the implanted engineered lung lobes. In line with the recently proposed repopulation index [46], we suggest that the quantitative user-independent approach described here for measuring the efficiency of the initial reseeding of a decellularized lung, may be also useful for evaluating later time points of the recellularization processes. Furthermore, the rationale, methodology and concepts developed here may be adapted to studying the repopulation of other decellularized organs and/or synthetic scaffolds. Our study highlights two important components of successful whole organ bioengineering, namely the need to i) match at a molecular level the profile of integrin receptors on the target cell and the binding motifs on the scaffold and ii) evaluate at a macro level the distribution and organization of the seeded cells throughout the recellularized organ.

5. Conclusions

In this study, we present a fresh and rational approach for improving recellularization of decellularized lung scaffolds for whole lung tissue engineering. Our approach is based on the analysis of the specific interactions between integrin receptors of the target cells to be seeded and ECM proteins composition of the scaffold. By pre-incubating the decellularized lungs with A549 cells-derived CM, we were able to regenerate a functional lung matrix with enhanced adhesive properties for mESCs. Medium conditioned by A549 cells contains FN and copious amounts of lung-specific LM 511, both of which were efficiently adsorbed into the decellularized lung matrix upon pre-treatment with the CM. Mouse ESCs express integrin receptors $\alpha 3\beta 1/\alpha 6\beta 1$ and $\alpha 5\beta 1$, which can effectively bind LM 511 and FN, respectively, and demonstrate enhanced initial binding upon reseeding into CM-treated decellularized whole lung. This finding stresses the importance to match the integrin receptor repertoire of the cells and the cell binding motifs on scaffolds in general and the ECM of the decellularized lung matrices, in particular. Our approach to functionalize the decellularized matrix by pre-treating with CM may have further implications for enhancing lung-specific differentiation of the stem cells *in situ* upon reseeding in optimized decellularized lung scaffold. Of particular interest will be to evaluate the CM as single component for both functionalization of the scaffold and induction of differentiation, thus potentially simplifying the bioprocess for *ex vivo* whole lung organ engineering (currently under investigation in our laboratory).

Author Manuscript Author Manuscript Author Manuscript Author Manuscript

Supplementary Material

Refer to Web version on PubMed Central for supplementary material.

Acknowledgments

PIL is the Laura H. Carnell Professor for Bioengineering; CTS is a NASA graduate student research program (GSRP) fellow. The authors acknowledge Ms. Zehava Cohen for graphics design.

References

1. Hertz MI. The Registry of the International Society for Heart and Lung Transplantation–Introduction to the 2012 annual reports: new leadership, same vision. J Heart Lung Transplant. 2012; 31:1045–51. [PubMed: 22975094]
2. Song JJ, Ott HC. Bioartificial lung engineering. Am J Transplant. 2012; 12:283–8. [PubMed: 22026560]
3. Crapo PM, Gilbert TW, Badylak SF. An overview of tissue and whole organ decellularization processes. Biomaterials. 2011; 32:3233–43. [PubMed: 21296410]
4. Wagner DE, Bonvillain RW, Jensen T, Girard ED, Bunnell BA, Finck CM, et al. Can stem cells be used to generate new lungs? Ex vivo lung bioengineering with decellularized whole lung scaffolds. Respirology. 2013; 18:895–911. [PubMed: 23614471]
5. Arenas-Herrera JE, Ko IK, Atala A, Yoo JJ. Decellularization for whole organ bioengineering. Biomed Mater. 2013; 8:014106. [PubMed: 23353764]
6. Geiger B, Spatz JP, Bershadsky AD. Environmental sensing through focal adhesions. Nat Rev Mol Cell Biol. 2009; 10:21–33. [PubMed: 19197329]
7. Marcinkiewicz C. Applications of snake venom components to modulate integrin activities in cell-matrix interactions. Int J Biochem Cell Biol. 2013; 45:1974–86. [PubMed: 23811033]
8. Prokhorova TA, Rigbolt KT, Johansen PT, Henningsen J, Kratchmarova I, Kassem M, et al. Stable isotope labeling by amino acids in cell culture (SILAC) and quantitative comparison of the membrane proteomes of self-renewing and differentiating human embryonic stem cells. Mol Cell Proteomics. 2009; 8:959–70. [PubMed: 19151416]
9. Caccia D, Zanetti Domingues L, Micciche F, De Bortoli M, Carniti C, Mondellini P, et al. Secretome compartment is a valuable source of biomarkers for cancer-relevant pathways. J Proteome Res. 2011; 10:4196–207. [PubMed: 21751813]
10. Roszell B, Mondrinos MJ, Seaton A, Simons DM, Koutzaki SH, Fong GH, et al. Efficient derivation of alveolar type II cells from embryonic stem cells for in vivo application. Tissue Eng Part A. 2009; 15:3351–65. [PubMed: 19388834]
11. Siti-Ismail N, Samadikuchaksaraei A, Bishop AE, Polak JM, Mantalaris A. Development of a novel three-dimensional, automatable and integrated bio-process for the differentiation of embryonic stem cells into pulmonary alveolar cells in a rotating vessel bioreactor system. Tissue Eng Part C Meth. 2012; 18:263–72.
12. Tuszynski GP, Srivastava S, Switalska HI, Holt JC, Cierniewski CS, Niewiarowski S. The interaction of human platelet thrombospondin with fibrinogen. Thrombospondin purification and specificity of interaction. J Biol Chem. 1985; 260:12240–5. [PubMed: 3930491]
13. Marcinkiewicz C, Vijay-Kumar S, McLane MA, Niewiarowski S. Significance of RGD loop and C-terminal domain of echistatin for recognition of alphaIIb beta3 and alpha(v) beta3 integrins and expression of ligand-induced binding site. Blood. 1997; 90:1565–75. [PubMed: 9269775]
14. Lecht S, Arien-Zakay H, Wagenstein Y, Inoue S, Marcinkiewicz C, Lelkes PI, et al. Transient signaling of Erk1/2, Akt and PLCgamma induced by nerve growth factor in brain capillary endothelial cells. Vasc Pharmacol. 2010; 53:107–14.
15. Marcinkiewicz C, Rosenthal LA, Mosser DM, Kunicki TJ, Niewiarowski S. Immunological characterization of eristostatin and echistatin binding sites on alpha IIb beta 3 and alpha V beta 3 integrins. Biochem J. 1996; 317(Pt 3):817–25. [PubMed: 8760368]

Author Manuscript Author Manuscript Author Manuscript Author Manuscript

16. Koharski, CD.; Lelkes, PI. Acellularized murine myocardium as a tissue-specific scaffold for cardiac tissue engineering. Philadelphia, PA: Drexel University; 2005.
17. Parameswaran H, Bartolak-Suki E, Hamakawa H, Majumdar A, Allen PG, Suki B. Three-dimensional measurement of alveolar airspace volumes in normal and emphysematous lungs using micro-CT. J Appl Phys. 2009; 107:583–92.
18. Pimton P, Sarkar S, Sheth N, Perets A, Marcinkiewicz C, Lazarovici P, et al. Fibronectin-mediated upregulation of alpha5beta1 integrin and cell adhesion during differentiation of mouse embryonic stem cells. Cell Adh Migr. 2011; 5:73–82. [PubMed: 20962574]
19. Ohtsuka M, Ishii K, Kikuti YY, Warita T, Suzuki D, Sato M, et al. Construction of mouse 129/Ola BAC library for targeting experiments using E14 embryonic stem cells. Genes Genet Syst. 2006; 81:143–6. [PubMed: 16755138]
20. Nguyen NM, Senior RM. Laminin isoforms and lung development: all isoforms are not equal. Dev Biol. 2006; 294:271–9. [PubMed: 16643883]
21. Lecht S, Gerstenhaber JA, Stabler CT, Karamil S, Pimton P, Marcinkiewicz C, et al. Heterogenic mixed-lineage differentiation of embryonic stem cells differentiated with A549 conditioned media. Stem Cells Dev. submitted.
22. Sroka IC, Chen ML, Cress AE. Simplified purification procedure of laminin-332 and laminin-511 from human cell lines. Biochem Biophys Res Commun. 2008; 375:410–3. [PubMed: 18713621]
23. Pierce JA, Hocott JB. Studies on the collagen and elastin content of the human lung. J Clin Invest. 1960; 39:8–14. [PubMed: 14432825]
24. Jensen T, Roszell B, Zang F, Girard E, Matson A, Thrall R, et al. A rapid lung de-cellularization protocol supports embryonic stem cell differentiation in vitro and following implantation. Tissue Eng Part C Meth. 2012; 18:632–46.
25. Hohenester E, Engel J. Domain structure and organisation in extracellular matrix proteins. Matrix Biol. 2002; 21:115–28. [PubMed: 11852228]
26. Daly AB, Wallis JM, Borg ZD, Bonvillain RW, Deng B, Ballif BA, et al. Initial binding and recellularization of decellularized mouse lung scaffolds with bone marrow-derived mesenchymal stromal cells. Tissue Eng Part A. 2012; 18:1–16. [PubMed: 21756220]
27. Thiesse J, Namati E, Sieren JC, Smith AR, Reinhardt JM, Hoffman EA, et al. Lung structure phenotype variation in inbred mouse strains revealed through in vivo micro-CT imaging. J Appl Phys. 2010; 109:1960–8.
28. He M, Callanan A. Comparison of methods for whole-organ decellularization in tissueengineering ofbioartificial organs. TissueEng PartB Rev. 2013; 19:194–208.
29. Rahmany MB, Van Dyke M. Biomimetic approaches to modulate cellular adhesion in biomaterials: a review. Acta Biomater. 2013; 9:5431–7. [PubMed: 23178862]
30. Lee ST, Yun JI, Jo YS, Mochizuki M, van der Vlies AJ, Kontos S, et al. Engineering integrin signaling for promoting embryonic stem cell self-renewal in a precisely defined niche. Biomaterials. 2010; 31:1219–26. [PubMed: 19926127]
31. Hayashi Y, Furue MK, Okamoto T, Ohnuma K, Myoishi Y, Fukuhara Y, et al. Integrins regulate mouse embryonic stem cell self-renewal. Stem Cells. 2007; 25:3005–15. [PubMed: 17717067]
32. Wallis JM, Borg ZD, Daly AB, Deng B, Ballif BA, Allen GB, et al. Comparative assessment of detergent-based protocols for mouse lung de-cellularization and re-cellularization. Tissue Eng Part C Meth. 2012; 18:420–32.
33. Garcia AJ, Vega MD, Boettiger D. Modulation of cell proliferation and differentiation through substrate-dependent changes in fibronectin conformation. Mol Biol Cell. 1999; 10:785–98. [PubMed: 10069818]
34. Graslund S, Nordlund P, Weigelt J, Hallberg BM, Bray J, Gileadi O, et al. Protein production and purification. Nat Meth. 2008; 5:135–46.
35. Koukoulis GK, Warren WH, Virtanen I, Gould VE. Immunolocalization of integrins in the normal lung and in pulmonary carcinomas. Hum Pathol. 1997; 28:1018–25. [PubMed: 9308725]
36. Kleinman HK. Preparation of basement membrane components from EHS tumors. Curr Protoc Cell Biol. 2001; Chapter 10(Unit 10):2.
37. Soto-Gutierrez A, Zhang L, Medberry C, Fukumitsu K, Faulk D, Jiang H, et al. A whole-organ regenerative medicine approach for liver replacement. Tissue Eng Part C Meth. 2011; 17:677–86.

Author Manuscript Author Manuscript Author Manuscript Author Manuscript

38. Girard ED, Jensen TJ, Vadasz SD, Blanchette AE, Zhang F, Moncada C, et al. Automated procedure for biomimetic de-cellularized lung scaffold supporting alveolar epithelial transdifferentiation. Biomaterials. 2013; 34:10043–55. [PubMed: 24095252]
39. Crisanti MC, Koutzaki SH, Mondrinos MJ, Lelkes PI, Finck CM. Novel methods for delivery of cell-based therapies. J Surg Res. 2008; 146:3–10. [PubMed: 17686493]
40. Fernandez Tena A, Casan Clara P. Deposition of inhaled particles in the lungs. Arch Bronconeumol. 2012; 48:240–6. [PubMed: 22464044]
41. Namati E, Chon D, Thiesse J, Hoffman EA, de Ryk J, Ross A, et al. In vivo micro-CT lung imaging via a computer-controlled intermittent iso-pressure breath hold (IIBH) technique. Phys Med Biol. 2006; 51:6061–75. [PubMed: 17110770]
42. Mosher DF, Fogerty FJ, Chernousov MA, Barry EL. Assembly of fibronectin into extracellular matrix. Ann N Y Acad Sci. 1991; 614:167–80. [PubMed: 1673833]
43. Petersen TH, Calle EA, Zhao L, Lee EJ, Gui L, Raredon MB, et al. Tissue-engineered lungs for in vivo implantation. Science. 2010; 329:538–41. [PubMed: 20576850]
44. Ott HC, Clippinger B, Conrad C, Schuetz C, Pomerantseva I, Ikonomou L, et al. Regeneration and orthotopic transplantation of a bioartificial lung. Nat Med. 2010; 16:927–33. [PubMed: 20628374]
45. Song JJ, Kim SS, Liu Z, Madsen JC, Mathisen DJ, Vacanti JP, et al. Enhanced in vivo function of bioartificial lungs in rats. Ann Thorac Surg. 2011; 92:998–1005. discussion-6. [PubMed: 21871290]
46. Sun, H.; Calle, EA.; Chen, X.; Mathur, A.; Zhu, Y.; Mendez, J., et al. Fibroblast engraftment in the decellularized mouse lung occurs via a beta1 integrin dependent, FAK dependent pathway that is mediated by ERK and opposed by AKT. Am J Physiol Lung Cell Mol Physiol. 2013. http://dx.doi.org/10.1152/ajplung.00100.2013

Appendix A. Supplementary data

Supplementary data related to this article can be found at http://dx.doi.org/10.1016/j.biomaterials.2013.12.093.

Author Manuscript Author Manuscript Author Manuscript Author Manuscript

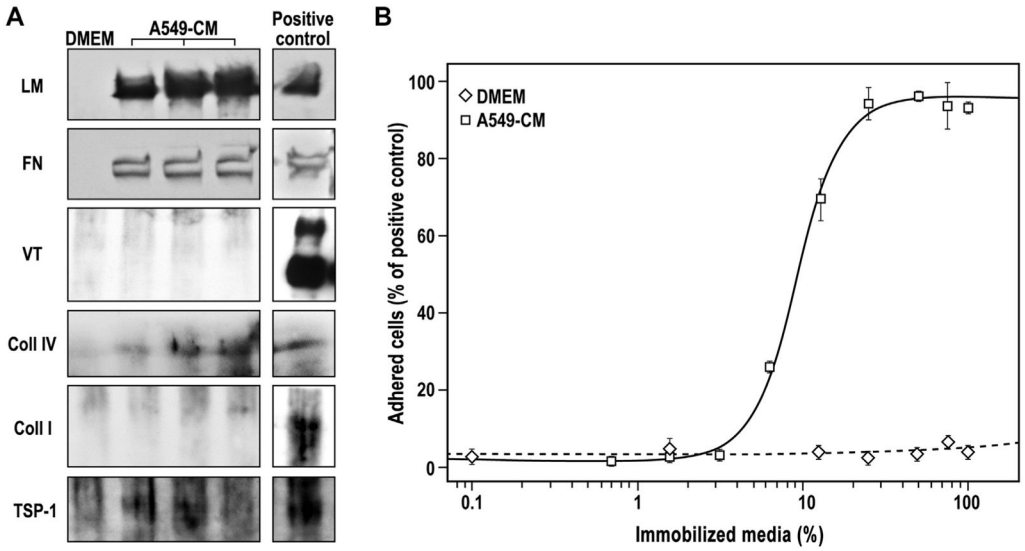

Fig. 1.

Composition and pro-adhesive activity of A549-CM. (A) Western blotting images of DMEM, three different batches of A549-CM and 1 μg/lane of purified ECM protein (Positive control). Antibodies used recognized: laminin (LM), fibronectin (FN), vitronectin (VT), collagen type IV (Coll IV), collagen type I (Coll I) and thrombospondin (TSP-1). (B) Adhesion of mESCs on increasing percentage of immobilized DMEM (white diamond) and A549-CM (white squares). The data are presented as the percentage of cells adhering to 1 μg/well of immobilized FN, which served as positive control. The adhesion to A549-CM was fitted using four-parameters logistic curve (R^2 = 0.9928). The data are mean ± SEM of at least three independent experiments in triplicate.

Author Manuscript Author Manuscript Author Manuscript Author Manuscript

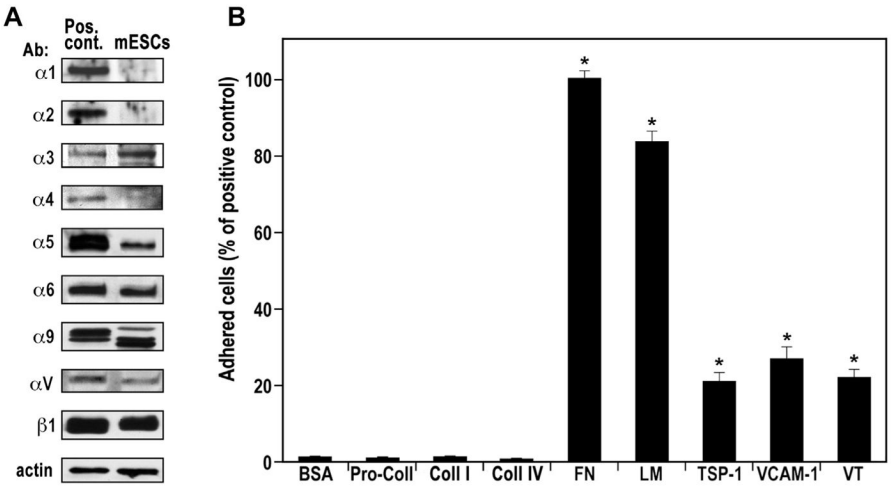

Fig. 2.

Functional expression of integrin receptors by mESCs. (A) Western blotting images of total cellular protein and positive control cells (Pos. Cont.). The corresponding specificity of each antibody used (Ab) is indicated on the left side of each image. The experiments were performed with at least three different passages of the mESCs yielding similar results; representative blots are presented. (B) Adhesion of mESCs on immobilized 1 μg/well of bovine serum albumin (BSA); collagen type IV (Coll IV); pro-collagen type I (Pro-Coll I); collagen type I (Coll I); fibronectin (FN, positive control set to 100%); laminin (LM); thrombospondin-1 (TSP-1); vascular cell adhesion molecule-1 (VCAM-1); and vitronectin (VT). The data are mean ± SEM of at least four independent experiments in triplicate. *$p <$ 0.01 vs. BSA.

Author Manuscript Author Manuscript Author Manuscript Author Manuscript

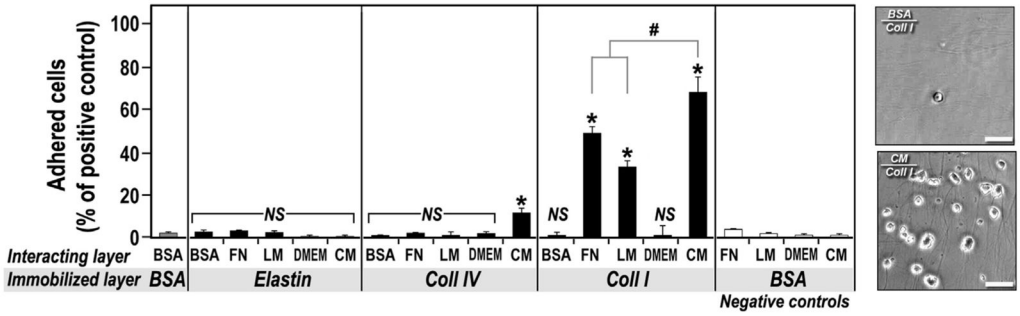

Fig. 3.

Adhesion of mESCs following CM-derived ECM–ECM interaction. Adhesion of mESCs in a two-layer experimental setup. Immobilized layer –1 μg/well of bovine serum albumin (BSA), elastin, collagen type IV (Coll IV) and collagen type I (Coll I) immobilized overnight on high-capacity binding plates; Interacting layer –incubation of 1 μg/well of BSA, fibronectin (FN), laminin (LM), and 100 μl of 100% DMEM and 100% CM for 1 h in the wells containing the immobilized ECM proteins. The data are presented as percentage of cells adhering to 1 μg/well of immobilized FN. The data are mean ± SD of three independent experiments in triplicate. *$p < 0.05$ vs. BSA/BSA; #$p < 0.05$ vs. CM/Coll I; *NS* –not significant vs. BSA/BSA. Right panel –representative photomicrographs of mESC adhering to immobilized Coll I overlaid with BSA (negative control) or CM. Phase contrast photomicrographs were acquired at 200× magnification, scale bar –50 μm.

Author Manuscript Author Manuscript Author Manuscript Author Manuscript

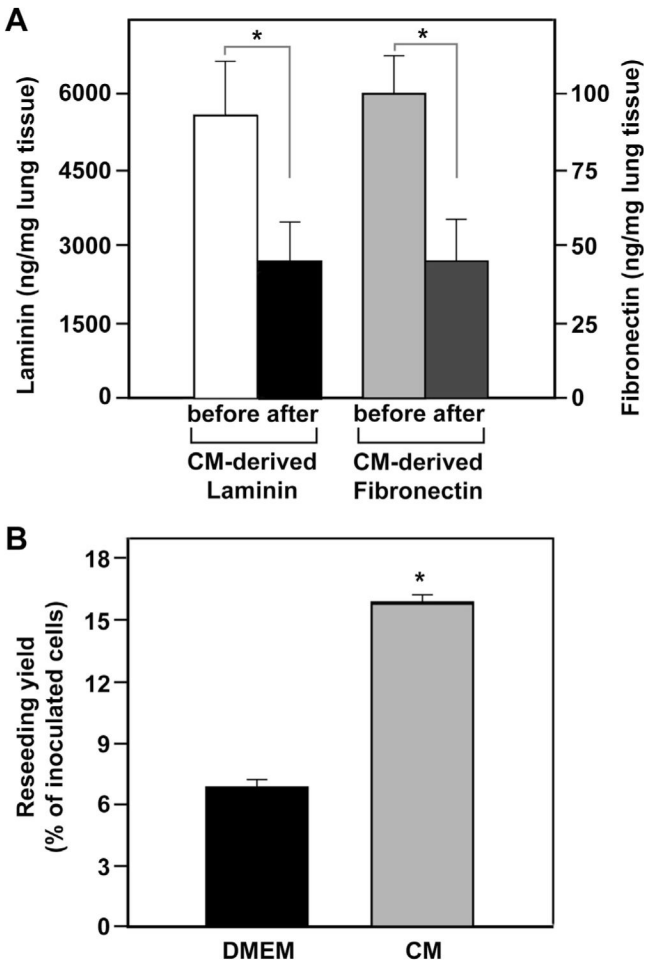

Fig. 4.

Adsorption of CM-derived ECM proteins and mESCs repopulation of decellularized lungs. (A) Quantitation of laminin and fibronectin in CM before and after incubation with decellularized lung slices using specific ELISA. The data represent the amounts of ECM proteins in ng/mg of supernatants normalized to dry weight of decellularized lung tissue. The data are mean ± SD of three independent experiments in triplicate. *$p < 0.05$ after vs. before. (B) Quantitation of fluorescently-labeled mESCs retained upon repopulation in the decellularized lungs pre-treated with DMEM or CM. The fluorescent dye was extracted and the number of retained cells was determined using calibration curves of known cell numbers. The data are presented as the percentage of mESCs specifically adhered in the left lobe of the total inoculated cell number. The data are mean ± SEM of eight reseeded left lobes. *$p <$ 0.05 CM vs. DMEM.

Author Manuscript Author Manuscript Author Manuscript Author Manuscript

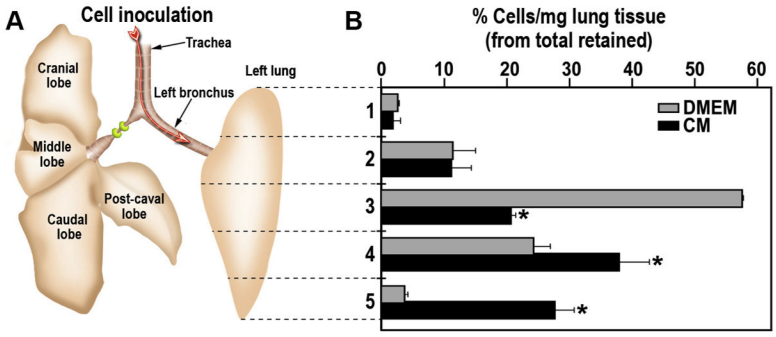

Fig. 5.

Longitudinal distribution of mESCs upon inoculation into decellularized lung. (A) Schematic presentation of the rat lungs with right main bronchus ligated and mESCs inoculated via the trachea into left lobe. Dashed lines indicate the location of the sections made to generate five distinct areas along the cranial-caudal axis. (B) Fluorescently-labeled mESCs were gravitationally inoculated into DMEM (gray bars) or CM (black bars) pre-treated lobes. Following 1 h incubation the left lobes were sectioned along the dashed lines, the sections were solubilized and the cell numbers was quantitated as per the calibration curves. The data are presented as the percentage of total cell number retained in the lobe normalized to the weight of the dry tissue. The data are mean ± SEM of six reseeded left lobes. *$p < 0.05$ CM vs. DMEM.

Author Manuscript Author Manuscript Author Manuscript Author Manuscript

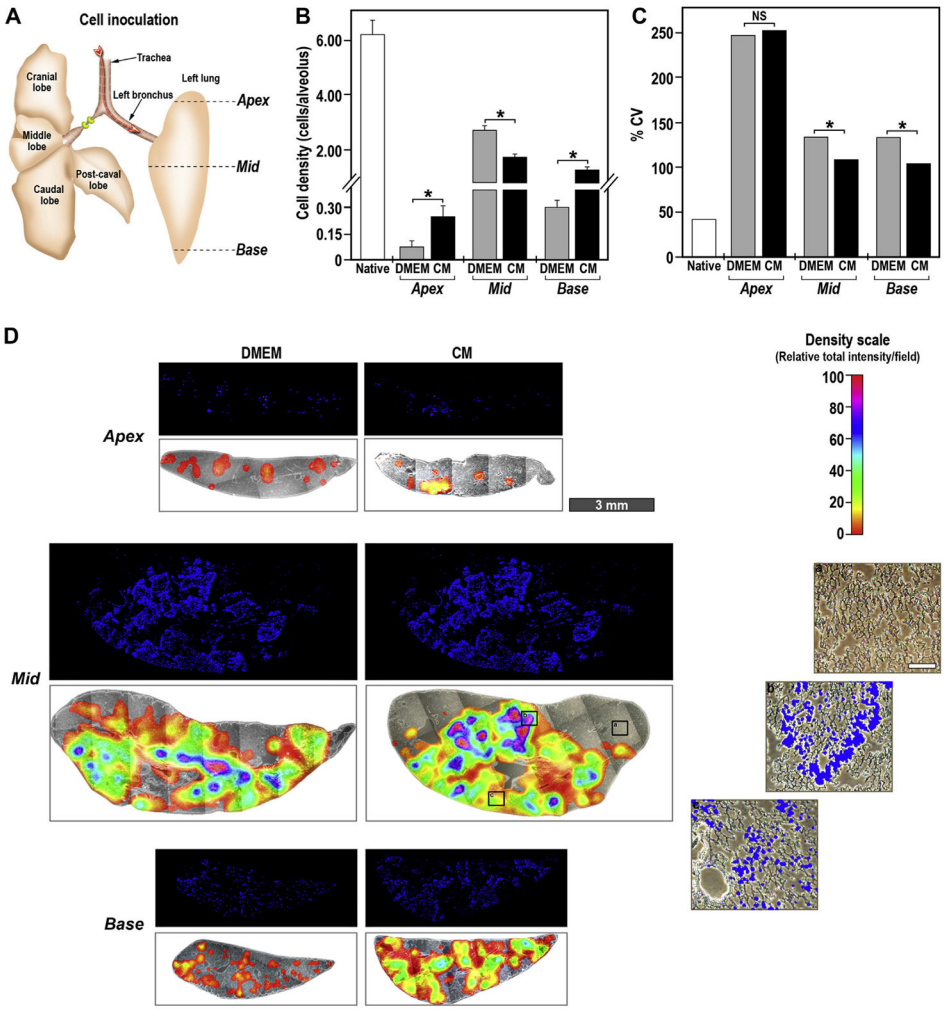

Fig. 6.

Transversal distribution of mESCs upon inoculation into decellularized lung. (A) Schematic presentation of the rat lungs with right main bronchus ligated and the mESCs inoculated via trachea into left lobe. The solid lines designated as apex, mid and base indicate the localization of transversal histological slices. (B) Average number of nuclei per field of the grid of repopulated decellularized lungs pre-treated with DMEM (gray bars) and CM (black bars) expressed as cell number per alveolus. The experiments were performed with three independently repopulated lobes with essentially similar results. The data are mean ± SEM of a representative analysis. Unpaired *t*-test with Welch correction was performed to calculate the two tailed *p*-values, $*p < 0.01$ for CM vs. DMEM. (C) Coefficient of variation (%CV) as calculated from the average cell density in (B). NS –not significant, $*p < 0.05$ for CM vs. DMEM. (D) Histological slice of reseeded DMEM- or CM-coated lobes were prepared and mounted in DAPI-containing mounting solution. Fluorescent (blue –DAPI staining) and phase-contrast photomicrographs were stitched using 4.2× objective to obtain an image of the whole slice. The phase-contrast photomicrographs are overlayed with representative density maps of relative fluorescent signal intensity per field of the grid of the corresponding fluorescent image. The color scale is in arbitrary units to maximize the

relative mean signal difference in each slice (Density scale) from 0 (transparent) until 100 (red), (scale bar –3 mm). (a), (b) and (c) are phase-contrast photomicrographs overlayed with DAPI fluorescence from the indicated areas on the CM-treated Mid section at 100× magnification (scale bar –100 μm).

Author Manuscript Author Manuscript Author Manuscript Author Manuscript

Author Manuscript

Author Manuscript

Author Manuscript

Author Manuscript

Table 1

Potency and efficacy of mESCs adhesion to ECM proteins.

ECM protein	Potency (EC_{50})	Efficacy	R^2
Fibronectin	11.6 ± 0.4	97.8 ± 1.0%	0.9778
Vitronectin	1275.3 ± 29.0	84.9 ± 1.4%	0.9943
Thrombospondin-1	607.0 ± 5.3	42.6 ± 1.1%	0.9878
LM 511	72.2 ± 2.4	111.0 ± 1.4%	0.9960
LM 521	77.9 ± 6.2	97.7 ± 1.5%	0.9870
LM 332	177.7 ± 16.4	100 ± 3.2%	0.9802
LM 421	202.6 ± 13.6	86.1 ± 2.0%	0.9883
LM 211	409.7 ± 29.4	93.2 ± 2.9%	0.9840
LM 111	504.4 ± 55.2	67.7 ± 2.0%	0.9769
LM 411	947.9 ± 92.0	101.7 ± 5.5%	0.9852

Potency is expressed as EC_{50} (ng/well) of the immobilized proteins and efficacy is expressed as the percentage cells adhered in comparison to adhesion to the positive control (1 μg/well of immobilized fibronectin). The data are mean ± SEM of three independent experiments performed in triplicates ($n = 9$). R^2 is the correlation coefficient of the four parameters logistic curve fitted to calculate the potency and efficacy. LM –laminin.